Available online at www.sciencedirect.com

ScienceDirect

Energy Procedia 48 (2014) 394 – 404

Energy Procedia

SHC 2013, International Conference on Solar Heating and Cooling for Buildings and Industry
September 23-25, 2013, Freiburg, Germany

Experimental studies of the mechanism and kinetics of hydration reactions

Kirsten Linnow[a], Michael Niermann[a], Dennis Bonatz[a], Konrad Posern[b], Michael Steiger[a]

[a]*Department of Chemistry, University of Hamburg, Inorganic and Applied Chemistry, Martin-Luther-King-Platz 6, 20146 Hamburg, Germany*
[b]*Bauhaus-University Weimar, Chair of Building Chemistry, Coudraystraße 13C, 99421 Weimar, Germany*

Abstract

The mechanism and the kinetics of hydration reactions are important for the application of a salt hydrate as a thermochemical heat storage material. $MgSO_4 \cdot H_2O$ and Na_2SO_4 were chosen in this study because they are both promising candidates for such an application. Considering that the hydration of these salts yields $MgSO_4 \cdot 7H_2O$ and $Na_2SO_4 \cdot 10H_2O$ as the reaction products, the maximum overall heat effect can be calculated from the heat of condensation of water vapor (44 kJ mol^{-1}) and the heats of hydration of 75 kJ·mol^{-1} (for $MgSO_4 \cdot H_2O$) and 81 kJ mol^{-1} (for Na_2SO_4). Based on the densities of the two hydrated phases, this results in the very high theoretical energy densities of 2.3 GJ·m^{-3} and 2.4 GJ·m^{-3}, respectively, for $MgSO_4 \cdot 7H_2O$ and $Na_2SO_4 \cdot 10H_2O$. Not only the energy density is important for the dimensioning of a storage system, but also the kinetics of hydration reactions play a major role for the application as storage material. In the present study, hydration reactions under varying climatic conditions were investigated by using water vapor sorption measurements and in-situ Raman microscopy. Using the phase diagrams, it can be clearly shown that the mechanism and the kinetics depend on the climatic conditions. Below the deliquescence humidity of the lower hydrated phase the hydration proceeds as solid state reaction, whilst above the deliquescence humidity a through solution mechanism takes place.

Selection and peer review by the scientific conference committee of SHC 2013 under responsibility of PSE AG

Keywords: thermochemical heat storage, hydration mechanism, magnesium sulfate; sodium sulfate

1. Introduction

Salt hydrates and water adsorbents are of increasing interest as storage materials for low potential heat (e.g. solar energy) [1−5]. These storage materials are charged by heat induced dehydration of the salt hydrate or desorption of the adsorbents. Thereafter, the stored heat is released by hydration of the salt or vapor sorption of the adsorbents. Water uptake is controlled by the relative humidity (*RH*) and temperature of the environment, i.e. by the water vapor

1876-6102
Selection and peer review by the scientific conference committee of SHC 2013 under responsibility of PSE AG
doi:10.1016/j.egypro.2014.02.046

partial pressure. A salt absorbs moisture from the air if the relative humidity exceeds the equilibrium humidity for the hydration–dehydration reaction or the deliquescence humidity (DRH) at a given temperature. At relative humidities between the equilibrium humidity for the hydration–dehydration reaction and the DRH, the salt picks up water vapor forming a higher hydrated state. Above the DRH the salt dissolves until reaching equilibrium, i.e. until the water activity of the solution is equal to the relative humidity.

Due to the high theoretical heat of reaction of 334.2 $kJ \cdot mol^{-1}$ [6] for the hydration of $MgSO_4 \cdot H_2O$ with water vapor and formation of $MgSO_4 \cdot 7H_2O$ i.e. an energy density of 2.30 $GJ \cdot m^{-3}$, first investigations were carried out in the system $MgSO_4$–H_2O. It turned out that the hydration did not lead to the expected thermodynamically stable product $MgSO_4 \cdot 7H_2O$. $MgSO_4 \cdot 6H_2O$ was found as the main reaction product instead [7]. Kinetic hindrance was also observed by other authors [8,9,10] and, though not yet fully understood, it appears plausible that diffusive water transport across a barrier product layer formed at the reaction interface may often be the rate limiting step. However, at high humidities above the deliquescence humidity of the lower hydrated phase a complete hydration can be achieved presumably accompanied by a change in the mechanism [9]. However, as yet, a systematic investigation of the hydration behavior is not available, and, therefore, the hydration of bulk $MgSO_4 \cdot H_2O$ was investigated at different humidities in the present work using water vapor sorption measurements and *RH* and *T* controlled Raman microscopy. Additional experiments were carried out with Na_2SO_4 for two reasons. First, the theoretical heat of reaction of 522 $kJ \cdot mol^{-1}$ (based on data provided in ref. [11]) results in a high energy density of 2.37 $GJ \cdot m^{-1}$ ($Na_2SO_4 \cdot 10H_2O$), hence, this salt is a promising heat storage material as well. The second reason is to confirm that the formation of a product barrier layer on the surface of the lower hydrate is a general feature responsible for the sluggish kinetics of hydration reactions.

It is well known that salt crystals often clump together during a hydration which leads to a lowering of the air flow rate through a heat storage tank, thus, severely hindering the release of the stored heat. To overcome this problem, experiments were carried out with salts dispersed in porous host materials [5], but the influence of the confinement on the hydration reaction is poorly investigated. In the present work, first investigations covering a broad range of pore sizes (1.7 µm to 7 nm in diameter) were carried out at 85 % *RH* and room temperature and the influence of the confinement is discussed.

2. Materials and methods

2.1. Salts

$MgSO_4 \cdot 6H_2O$ (Fluka 00627 p.a.) and Na_2SO_4 (Merck 1.06649 A.C.S.) were used as provided by the manufacturers. $MgSO_4 \cdot 7H_2O$ (Fluka 63140 p.a.) and $Na_2SO_4 \cdot 10H_2O$ (Merck 6648 p.A.) were stored for at least four weeks in a desiccator over saturated KCl solution, i.e. at 84 % *RH* to avoid dehydration at room conditions. As shown by Grindrod et al. [12] and Steiger et al. [13] the reagent-grade $MgSO_4$ monohydrate purchased from Fluka (63141 purum) largely consists of $MgSO_4 \cdot 1.25H_2O$. To prepare the pure monohydrate, the Fluka material was heated to 150 °C for about ten days. The identity of the $MgSO_4 \cdot H_2O$ phase was verified by X-ray powder diffraction (XRD) and comparison with JCPDS standard [14] PDF 33-882 ($MgSO_4 \cdot H_2O$).

2.2. Vapor sorption measurements

Dynamic vapor sorption measurements were made using a homemade setup with an analytical balance (Handy H51, Sartorius Mechatronics, Germany) as depicted in Fig. 1a. The windshield is replaced by an acrylic glass chamber with a volume of 800 mL. The mixing chamber (2a) of a humidity generator (1a) (MHG32, ProUmid GmbH, Germany) providing humid air at a flow rate of 500 $mL \cdot min^{-1}$, is connected to the humidity chamber. Impingement baffles were mounted close to the inlet and outlet ports to obtain a homogenous distribution of the humid air in the chamber. A capacitive humidity sensor (3a) (HycroClip, Rotronic, Switzerland) connected to the humidity generator is placed directly above the sample (4a). A computer program is used to control the humidity in the chamber. To ensure a constant specific surface area, the samples were sieved and the sieve fraction of 40−63 µm was used in the vapor sorption experiments.

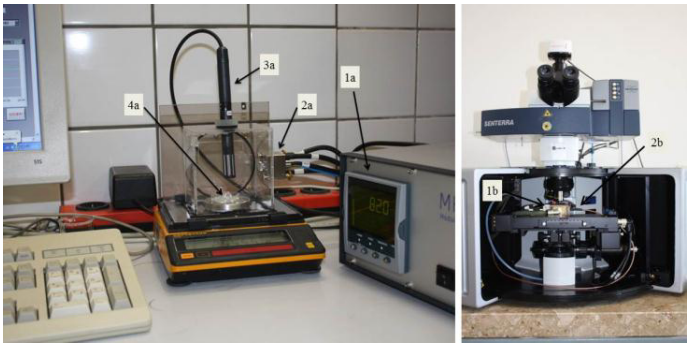

Fig. 1: (a) Dynamic vapor sorption analyzer with modular humidity generator (1a) connected to the mixing chamber (2a) and to the climatic chamber of the balance H51 (Sartorius, Germany). The humidity sensor (3a) is placed directly above the sample (4a). (b) Senterra Raman dispersive microscope equipped with a thermostated humidity chamber (1b); the humidity sensor (2b) is placed directly beside the sample in the chamber.

Samples of approximately 200 mg (bulk samples) and 600 mg (glass samples impregnated with $MgSO_4$ solution) were weighed into glass dishes and stored at 20 % *RH* and room temperature (21–26 °C). The hydration reaction was started by increasing the relative humidity to 85 % in a single step. Care was taken to achieve an even distribution of the grains on the bottom of the dishes to avoid stratification.

The moisture sorption was measured at constant humidities over a period of 24 to 25 h. For the bulk samples different humidities were chosen, whereas the impregnated glasses were measured only at 85 % *RH*. Sample mass and the climatic conditions in the chamber were continuously recorded every minute during the measurements. After the sorption measurement the total water content of the impregnated glasses was determined by drying the samples in a muffle kiln at 500 °C. Subsequently, the salt content was determined by weight after multiple extraction of the samples with doubly distilled water and drying in a muffle kiln at 500 °C.

2.3. Raman measurements

Raman spectra were recorded on a Senterra Raman dispersive microscope (Bruker Optics GmbH, Germany) with an automated Raman frequency calibration system (SurCal technology). The laser was operated at 532 nm and 20 mW. The Raman microscope was equipped with a humidity chamber made of brass. Humid air at a flow rate of 500 $ml \cdot min^{-1}$ is provided by the humidity generator MHG32 (ProUmid GmbH, Germany) and humidity is controlled by a HycroClip C05 probe (Rotronic, Switzerland) placed directly besides the sample holder of glass. The temperature in the 20 mL chamber is controlled by a thermostat (F20, Julabo GmbH, Germany).

To observe the hydration reactions in-situ the lower hydrate was placed into the chamber at room temperature. The humidity was kept constant at about 10 % *RH* until temperature equilibrium was achieved. Subsequently, the humidity was increased in a single step to the desired value and the phase transition was observed continuously by successively recorded Raman spectra and microphotographs.

2.4. Porous host materials and impregnation

Crushed porous glasses VitraPOR® P5 (ROBU Glassfiltergeräte GmbH, Germany), Trisopor® (VitraBio GmbH, Germany), CPI glass (CPI ChemiePark Institut Bitterfeld, Germany) and Vycor® 7930 (Corning Incorporated, USA) were used as porous host materials. In addition, porous glass (BUW glass) was synthesized as described by Janowski and Enke [15]. The median pore diameters *d* of the materials are 1.7·µm, 173 nm, 45 nm and 96 nm and their specific volumes are 0.34 $cm^3 \cdot g^{-1}$, 0.72 $cm^3 \cdot g^{-1}$, 0.36 $cm^3 \cdot g^{-1}$, 0.23 $cm^3 \cdot g^{-1}$and 0.16 $cm^3 \cdot g^{-1}$ respectively. The pellet sizes of Trisopor®, BUW and CPI varied from 1–2 mm; the VitraPOR® P5 and Vycor® 7930 pellets were slightly larger with diameters of about 2–4 mm. To prepare the samples weighed amounts of each host material were impregnated with a solution of 1.2 mol $MgSO_4 \cdot kg^{-1}$ water and filtrated. Excess solution adhering to the glass surface

was carefully wiped-off to avoid precipitation of salt on the outer surface. Afterwards, the impregnated glasses were first dried at 40 °C for three days and then at 130 °C for 2 hours in a drying cabinet.

2.5. Phase equilibria

Given a salt of composition $M_{\nu M}X_{\nu X}{\cdot}nH_2O$ consisting of ν_M positive ions M, ν_X negative ions X and n molecules of water, the equilibrium constant K_{MX} of the dissolution reaction, i.e. the thermodynamic solubility product, is given by

$$\ln K_{MX} = \nu_M \ln m_M + \nu_X \ln m_X + \nu_M \ln \gamma_M + \nu_X \ln \gamma_X + n \ln a_w \quad (1)$$

where m_M, m_X, γ_M and γ_X represent the molalities and activity coefficients of the cations and anions, respectively, and a_w is the water activity, i.e. the equilibrium relative humidity above the saturated solution which equals the DRH of the salt. The equilibrium humidity RH_{AB} for a particular hydration-dehydration reaction, where the lower hydrate A (n_A molecules of hydration water) takes up $\Delta n = n_B – n_A$ molecules water for the formation of the higher hydrated state B (with n_B molecules of hydration water), is related to the thermodynamic solubility products of the two phases A and B by

$$\ln RH_{AB} = \frac{\ln K_A - \ln K_B}{\Delta n_{H_2O}} \quad (2)$$

Using the available experimental data and an electrolyte solution model, the complete phase diagrams for the systems Na_2SO_4–H_2O and $MgSO_4$–H_2O can be calculated as described in detail by Steiger et al. [13,16]. There exist several metastable phases in the two systems such as $Na_2SO_4{\cdot}7H_2O$, Na_2SO_4(III), a polymorph of anhydrous Na_2SO_4, and $MgSO_4$ hydrates with n = 1.25, 2, 3, 4 and 5. However, none of these metastable phases has been observed in the present hydration experiments. Hence, for sake of simplicity, we only consider the thermodynamically stable phases in the following discussion. The phase diagrams are depicted on the right hand side of Fig. 2. Red lines represent the DRH of the lower hydrates $MgSO_4{\cdot}H_2O$ (top right) and Na_2SO_4 (bottom right). The blue lines represent the DRH of the higher hydrated states $MgSO_4{\cdot}6H_2O$ and $Na_2SO_4{\cdot}10H_2O$, whereas the green line gives the DRH of $MgSO_4{\cdot}7H_2O$. The dashed extensions of these curves represent the DRH of lower hydrated phases under climatic conditions where a higher hydrated form is thermodynamically stable. The hydration-dehydration equilibria are represented by the black lines. It follows that $Na_2SO_4{\cdot}10H_2O$ is thermodynamically stable in the field limited by its deliquescence curve (blue line) and the hydration equilibrium curve (black line in Fig. 2). Hence, the maximum temperature for the hydration of the Na_2SO_4 is given by the invariant point at 32.4 °C. $MgSO_4{\cdot}7H_2O$ is the thermodynamic stable phase in the field limited by its deliquescence curve (green) and two hydration equilibrium curves (black lines). The maximum temperature for the hydration of $MgSO_4{\cdot}H_2O$ to $MgSO_4{\cdot}7H_2O$ is given by the invariant point at 48.0 °C. Above this temperature hydration to $MgSO_4{\cdot}7H_2O$ cannot be achieved. The stability field of $MgSO_4{\cdot}6H_2O$ is rather small and this salt cannot exist above 70.0 °C.

2.5.1. Influence of confinement

As discussed by Steiger and Linnow [17,18] the solubility is influenced by two competitive factors, both are described by Eq. (3).

$$\ln K = \ln K_\infty - \frac{\Delta \overline{V^o}}{RT} \Delta p + \frac{2\gamma_{cl} V_m}{r_c RT} \quad (3)$$

where K is the solubility product of a crystal with radius r_c at pressure p and K_∞ is the solubility product of an infinitely large crystal at standard pressure. $\Delta\bar{V}^\circ$ is the change in molar volume of the dissolution reaction, R is the gas constant, T the absolute temperature, γ_{cl} the surface energy of the crystal–solution interface and V_m the molar volume of the crystalline solid.

In an unsaturated pore, a wetting fluid shows a concave meniscus and the curvature of the interface results in a pressure drop (Δp) in the liquid phase, which can be calculated by the Laplace equation. Due to the decreasing pressure the solubility decreases and the equilibrium humidity above the saturated solution increases. On the other hand, the solubility is also influenced by crystal size. Due to a lack of accurate values of the crystal–liquid interfacial energy and due to the unknown crystal size, this influence can only be roughly estimated. Nonetheless, it is clear that there is a solubility increase with decreasing crystal size resulting in a decrease of the equilibrium humidity above the saturated solution, i.e. a decrease of the DRH.

3. Results and discussion

3.1. Water vapor sorption

The water uptake curves are shown in Fig. 2 (left). Water uptake is expressed as the number of moles of water per mole of anhydrous salt versus time. The climatic conditions during water vapor sorption are shown as the shaded regions in the corresponding RH/T diagrams on the right. The variability along the x-axis is the result of the room temperature fluctuations during the measurements. Variability along the *RH* axis represents the measurement uncertainty of the humidity sensor which does not exceed 1.5 % *RH* as estimated by repeated measurements of the equilibrium *RH* above solutions saturated with respect to $LiCl{\cdot}H_2O$, NaCl, $MgCl_2{\cdot}6H_2O$ and KCl at room temperature. Repeated measurements with saturated salt solutions also confirmed a uniform distribution of the *RH* in the chamber, between the humidity probe and the sample.

Both the water uptake rate and the resulting water content of the samples increase with increasing humidity. In the experiments with Na_2SO_4 carried out at humidities below the DRH of the salt only a slight water uptake was observed and formation of $Na_2SO_4{\cdot}10H_2O$ is extremely slow (red curves), although the decahydrate is the stable product under these conditions. One measurement was made just above the DRH of Na_2SO_4. In this case (green curve), the hydration rate is slightly increased but the hydration is still incomplete not exceeding a water uptake of 1.8 moles of water within 25 hours. In the experiments carried at higher *RH*, i.e. distinctly above the DRH of Na_2SO_4, the water uptake increases, however, complete hydration to $Na_2SO_4{\cdot}10H_2O$ is not achieved within 25 hours. It should be noted that an air flow rate of 500 $mL{\cdot}min^{-1}$ at 85 % *RH* provides a maximum of 42 $mg{\cdot}min^{-1}$ (2.3 $mmol{\cdot}min^{-1}$) water considering a maximum of 100 % *RH* at the inlet port. This is a sufficient to hydrate 200 mg Na_2SO_4 within about 12 minutes. Therefore, the observed slow hydration rates are not the result of transport limitation.

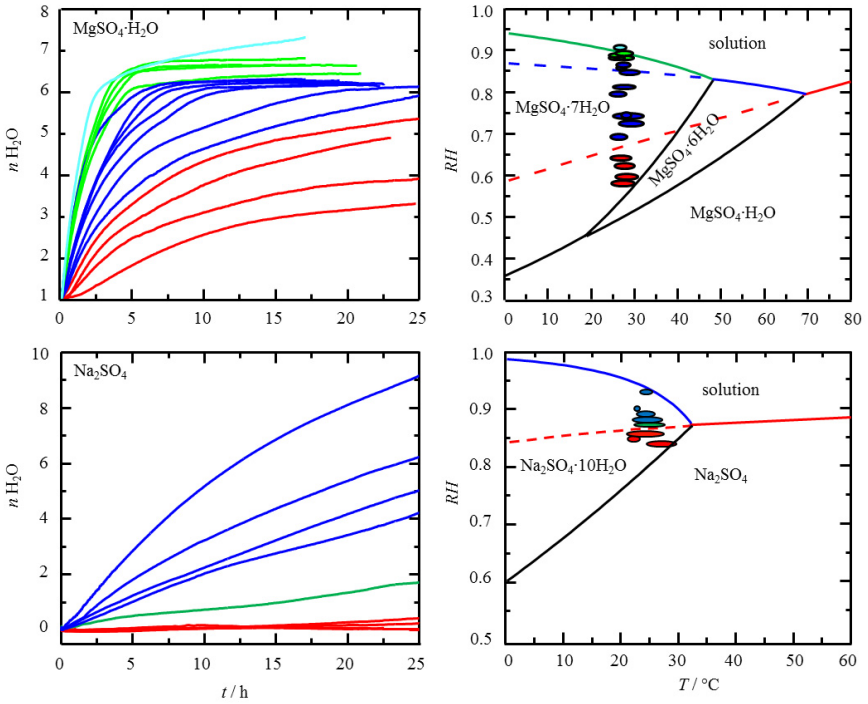

Fig. 2: Water uptake of $MgSO_4 \cdot H_2O$ (top left) and Na_2SO_4 (bottom left) expressed as the number of moles of water per mole $MgSO_4$ and Na_2SO_4, respectively. The shaded regions in the RH/T phase diagrams of the $MgSO_4$–H_2O (top right) and Na_2SO_4–H_2O (bottom right) systems represent the climatic conditions during water vapor sorption experiments. In the right diagrams, colored lines represent the DRH of $MgSO_4 \cdot H_2O$ (top right, red), $MgSO_4 \cdot 6H_2O$ (top right, blue), $MgSO_4 \cdot 7H_2O$ (top right, green), Na_2SO_4 (bottom right, red) and $Na_2SO_4 \cdot 10H_2O$ (bottom right, blue), ; dashed lines represent the DRH of lower hydrated states at climatic conditions where a higher hydrated form is thermodynamically stable; see text for the meaning of the colors of the water uptake curves.

The hydration behavior of $MgSO_4 \cdot H_2O$ as shown in Fig. 2 is more complex. The water uptake curves show that below the DRH of $MgSO_4 \cdot H_2O$ (red curves) a partial hydration and formation of $MgSO_4 \cdot 6H_2O$ takes place. The thermodynamically stable hydration product under these conditions is $MgSO_4 \cdot 7H_2O$. Full hydration to $MgSO_4 \cdot 6H_2O$ was not achieved within 60 hours (only the first 25 hours are shown in Fig. 2). Above the DRH of $MgSO_4 \cdot H_2O$ the hydration rate is significantly increased and the formation of $MgSO_4 \cdot 6H_2O$ is complete within 25 hours (blue curves). Partial formation of $MgSO_4 \cdot 7H_2O$ was only observed above the DRH of $MgSO_4 \cdot 6H_2O$ (green curves). Finally, a higher water uptake than 7 moles of water is observed slightly above the DRH of $MgSO_4 \cdot 7H_2O$ (light blue curve), thus, indicating the formation of a solution. The integral water uptake measurements reveal that hydration at humidities below the DRH of the lower hydrate is very slow and incomplete, whereas above the DRH a fast and complete hydration to $MgSO_4 \cdot 6H_2O$ is achieved. Similar results were also obtained in a previous investigation [9] where $MgSO_4 \cdot H_2O$ was dispersed in glass frits with a median pore diameter of d_m = 6 µm. Humidity and temperature controlled X-ray diffraction clearly confirmed [9] that the complete hydration to $MgSO_4 \cdot 6H_2O$ was only achieved above the deliquescence humidity of $MgSO_4 \cdot H_2O$, whereas the complete hydration to $MgSO_4 \cdot 7H_2O$ was only observed in a two steps reaction with initial formation of $MgSO_4 \cdot 6H_2O$. In accordance with Chipera and Vaniman [19] the direct hydration from monohydrate to heptahydrate was not oberserved.

For application as energy storage material it is important to note that the complete hydration to $MgSO_4 \cdot 7H_2O$ proceeds in two steps. Below the DRH of the hexahydrate the full theoretical storage potential cannot be achieved due to the formation $MgSO_4 \cdot 6H_2O$ instead of $MgSO_4 \cdot 7H_2O$. Hence, the theoretical storage density of 2.3 $GJ \cdot m^{-3}$ is reduced to 2.1 $GJ \cdot m^{-3}$. Only at humidities above the hexahydrate DRH, i.e. above about 85 % *RH* the complete hydration to the heptahydrate can be achieved.

Although visible water was not observed it is obvious that above the DRH deliquescence of the lower hydrate and subsequent crystallization takes place. This through-solution mechanism accelerates the hydration reaction significantly. Since the formation of a solution cannot be detected by XRD and since macroscopically visible amounts of solution were not observed during the water vapor sorption experiments, additional experiments using Raman microscopy were carried out.

3.2. Raman microscopy

To unambiguously identify the phases occurring during the water vapor sorption experiments, Raman reference spectra of all stable and metastable sodium sulfate hydrates and nearly all stable and metastable magnesium sulfate hydrates were recorded. The reference spectra are in a good agreement with available spectra in the literature [20–22]. Raman peak positions of the most intensive $\nu_1(SO_4^{2-})$ mode are compared in Table 1. Details of the preparation of the reference materials and the recording of the spectra are beyond the scope of the present paper and will be given elsewhere. As mentioned before, none the metastable hydrates of either Na_2SO_4 or $MgSO_4$ were observed in our hydration experiments, although the formation of such metastable phases is often observed during crystallization from solution and during dehydration [7,9,24]. An extensive discussion of the crystallization and dehydration behavior of the magnesium sulfate hydrates is provided by Steiger et al. [13].

Table 1: Raman peak positions (ν_1 mode) of magnesium sulfate hydrates and sodium sulfate hydrates

	ν_1 peak positions / cm^{-1}	
	this work	literature
SO_4^{-2} aquous	982.2 ± 0.4	982.1 [20]
$MgSO_4 \cdot 7H_2O$	984.7 ± 0.3	984.3 21]
$MgSO_4 \cdot 6H_2O$	984.5 ± 0.3	984.1 [21]
$MgSO_4 \cdot 5H_2O$	n.m.	1004.9 [21]
$MgSO_4 \cdot 4H_2O$	1000.5 ± 0.2	1000.3 [21]
$MgSO_4 \cdot 3H_2O$	n.m.	1023.8 [21]
$MgSO_4 \cdot 2H_2O$	n.m.	1033.8 [21]
$MgSO_4 \cdot 1.25H_2O$	1046.5 ± 0.3	
$MgSO_4 \cdot H_2O$	1043.5 ± 0.2	1046.1 [21]
Na_2SO_4	993.4 ± 0.4	993.2 [22]
Na_2SO_4 (Phase III)	996.7 ± 0.2	996.0 [23]
$Na_2SO_4 \cdot 7H_2O$	988.3 ± 0.2	987.6 [20]
$Na_2SO_4 \cdot 10H_2O$	989.8 ± 0.3	989.3 [20]

n.m. not measured

As an example, micrographs taken during the hydration of anhydrous Na_2SO_4 at 92 % *RH* and 23 °C are shown in Fig. 3. After an exposure time of nearly two hours (Fig. 3a) small Na_2SO_4 crystals started to dissolve by deliquescence (blue arrows) while larger crystals still remained in crystalline form (red arrows); the formation of $Na_2SO_4 \cdot 10H_2O$ was not yet observed. After about three hours, the hydration of the large crystals (green arrow in Fig. 3b) to $Na_2SO_4 \cdot 10H_2O$ takes place whereas medium sized crystals start to dissolve.

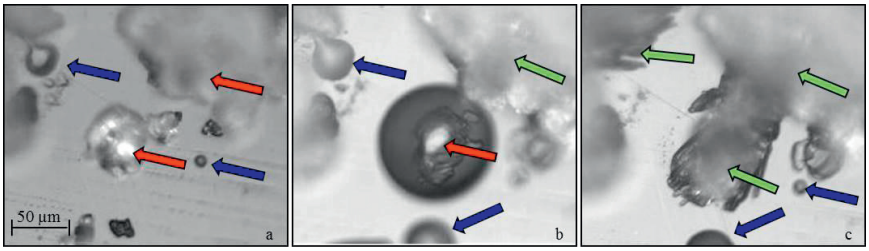

Fig. 3: Hydration of Na_2SO_4 at 92 % *RH* and 23 °C after exposure times of 2 h (a), 3 h (b) and 6 h (c). The arrows indicate the presence of Na_2SO_4 (red), $Na_2SO_4{\cdot}10H_2O$ (green) and of Na_2SO_4(aq) (blue) as detected by Raman spectroscopy.

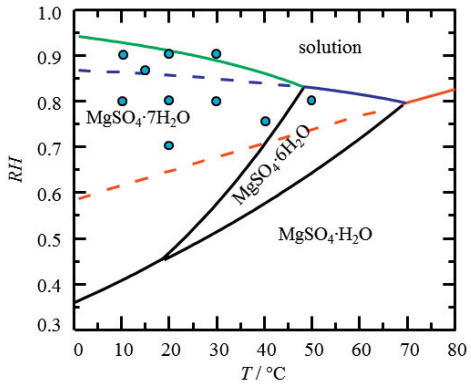

Fig. 4: Climatic conditions during the Raman microscopy experiments under which solution was detected are shown as blue points in the phase diagram.

In the interior of the large droplet (red arrow Fig. 3b) Na_2SO_4 is still visible and was identified by Raman spectroscopy. Shortly after the droplet got in contact with the $Na_2SO_4{\cdot}10H_2O$ particle spontaneous crystallization of $Na_2SO_4{\cdot}10H_2O$ occurred, thus providing evidence for a through-solution mechanism of hydration. After 6 hours, some droplets are still present and all crystals consist of $Na_2SO_4{\cdot}10H_2O$.

Similar results were found for the hydration of $MgSO_4{\cdot}H_2O$ which was observed under different humidities. Above the DRH of $MgSO_4{\cdot}H_2O$ both the formation of a solution and the direct hydration to $MgSO_4{\cdot}6H_2O$ was observed, whilst a solution was not formed below the DRH. The climatic conditions under which the formation of a solution was detected during the hydration of $MgSO_4{\cdot}H_2O$ are depicted in Fig. 4a. A through solution process was also observed using environmental scanning electron microscopy (ESEM) at 40 % RH and 2 °C by Balboni et al. [25]. The formation of $MgSO_4{\cdot}7H_2O$ was not observed within 6 hours. In conclusion, the Raman microscopy experiments provide evidence of the through-solution hydration mechanism above the DRH of the lower hydrated phases.

3.3. Water uptake in confined spaces

The water uptake of magnesium sulfate in various porous host materials was studied at 85 % *RH* and room temperature until the water content remains constant. The final water content after the hydration versus the median pore diameters of the host materials is depicted in Fig. 4b. It turns out that full hydration to the heptahydrate was not achieved in the largest pores (d_m = 1.7 µm). The water content in this sample is similar to the water content found previously in bulk samples [7]. In the smallest pores (d_m = 7 nm), the high water content indicates the formation of a solution which in turn is the result of capillary condensation. However, the water uptake of the $MgSO_4$ impregnated porous glass is significantly higher than that of the pure glass at the same *RH*. This increased water uptake is due to the salt dispersed in small pores. This is in accordance with the results of Simonova and Aristov [26], who found

that the adsorption of water by a calcium nitrate in silica gel is not the linear superposition of the adsorption properties of the host material and the bulk salt, i.e. synergism of properties is observed. The water content of magnesium sulfate in the medium sized pores (45–173 nm) also exceeds the water content of $MgSO_4 \cdot 7H_2O$, thus, indicating that both crystalline $MgSO_4$ hydrate (preferably the heptahydrate) and a $MgSO_4$ solution are present in these materials as well. Using the $MgSO_4$ content of the materials (listed as the weight ratio of the anhydrous salt in Table 2), the degree of pore filling after the hydration was estimated. Assuming that $MgSO_4$ is present as the heptahydrate, the sum of the solid phase volume and the volume of the solution formed by the excess water uptake was used for a rough estimate of the degree of pore space filling after exposure to the humid air. The results listed in Table 2 show that the pores are not fully saturated with solution. Therefore, the formation of menisci with concave curvature resulting in reduced pressure in the liquid phase is expected.

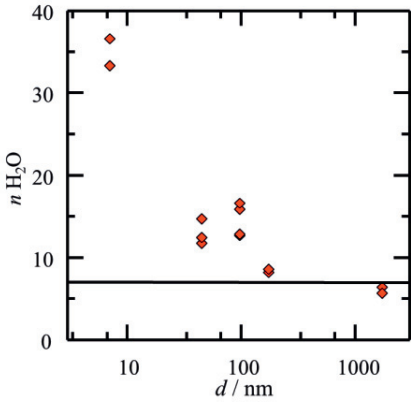

Fig. 5: Water content of the impregnated porous glasses (expressed as the number of moles of water per mole $MgSO_4$) versus median pore diameter. The dashed line represents the water content of $MgSO_4 \cdot 7H_2O$.

Supposing an equilibrium state in the pores, the *RH* above the solution in the pores has to be equal to the ambient *RH* of 85 % which is clearly below the value of 91 % for bulk $MgSO_4 \cdot 7H_2O$. As previously discussed, the influence of the decreased pressure due to the pore size results in increasing equilibrium humidity above the saturated solution. In contrast, a decreasing crystal size results in decreasing equilibrium humidity. Hence it is most likely that the formation of the solution in the medium sized pores is due to the influence of the crystal size.

Table 2: $MgSO_4$ content (given as weight ratio) of the impregnated porous glasses and degree of pore filling after exposure to humid air (85 % *RH*).

d / nm	$1.70 \cdot 10^3$	$1.70 \cdot 10^3$	173	173	96	96	96	96	45	45	45	7	7
weight ratio / %	7.4	7.5	14.8	16.1	4.8	4.6	5.4	4.8	10.5	10.2	8.5	4.2	4.6
pore filling / %	18	18	3	2	8	10	46	45	8	7	8	42	37

4. Conclusions

Water vapor sorption experiments show that hydration reactions are slow and incomplete if carried out below the DRH of the lower hydrate. As hydration starts at the crystal surface, a shell of the hydrated phase is formed around a core of the lower hydrated phase. Due to the volume expansion during hydration the product layer acts as a barrier layer hindering water vapor transport to the unhydrated core. Due the formation of a solution the hydration reaction is significantly accelerated above the DRH of the lower hydrate. In this case, the reaction proceeds via a two stage reaction pathway involving the deliquescence of the lower hydrate, i.e. formation of a solution, and subsequent crystallization of the higher hydrated phase. The present Raman experiments provide clear evidence for this through-solution mechanism.

Whilst the stable decahydrate is formed in the case of Na_2SO_4 hydration, the hydration of $MgSO_4 \cdot H_2O$ stopped at the stage of the hexahydrate. The stable product $MgSO_4 \cdot 7H_2O$ is only achieved if the reaction is carried out above the DRH of $MgSO_4 \cdot 6H_2O$. This result is important regarding the use of magnesium sulfate as energy storage material. The high theoretical storage density of 2.3 $GJ \cdot m^{-3}$ can only be achieved at sufficiently high relative humdities.

The influence of a confinement on the hydration of $MgSO_4 \cdot H_2O$ was investigated by using porous glasses with different pore diameters. It turns out that large pores (1.7 µm) do not have any significant influence on the hydration product and the kinetic hindrance of the $MgSO_4 \cdot 7H_2O$ formation could not be overcome. Capillary condensation and partial dissolution of the salt occurs in very small pores (7 nm) resulting in an increased water uptake compared to the pure host material. Solutions are also formed in materials with intermediate pore sizes (45–173 nm). This means that the equilibrium humidity of the solution present in these pores was less than or equal to the ambient *RH*. It was shown that most likely this is an influence of the crystal size.

Acknowledgements

Financial support by the Deutsche Forschungsgemeinschaft (DFG) is gratefully acknowledged. The authors thank G. W. Scherer (Princeton University) for supplying the Vycor® 7930. This work benefited a lot from helpful discussions with Dr. Felix Brieler (University of Hamburg).

References

[1] Jänchen J, Ackermann D, Stach H, Brösicke W. Studies of the water adsorption on zeolites and modified mesoporous materials for seasonal storage of solar heat, *Sol. Energy* 2004;76:339–344.

[2] Jänchen J, Ackermann D, Weiler E, Stach H, Brösicke W. Calorimetric investigations on zeolites, $AlPO_4$´s and $CaCl_2$ impregnated attapulgite for thermochemical storage of heat. *Thermochim. Acta* 2005;434:37–41.

[3] Levitskij E, Aristov YI, Tokarev M, Parmon V. Chemical heat accumulators, A new approach to accumulating low potential heat, *Sol. Energy Mater. Sol. Cells* 1996;44:219–235.

[4] Gordeeva LG, Grekova AD, Krieger TA, Aristov YI. Adsorption properties of composite materials (LiCl + LiBr)/silica, *Microporouros Mesoporous Mater.* 2009;126:262–267.

[5] Posern K, Kaps Ch. Calorimetric studies of thermochemical heat storage materials based on mixtures of $MgSO_4$ and $MgCl_2$. *Thermochim. Acta* 2010;502:73–76.

[6] Grevel KD, Majzlan J, Benisek A, Dachs E, Steiger M, Fortes AD, Marler B. Experimentally Determined Standard Thermodynamic Properties of Synthetic $MgSO_4 \cdot 4H_2O$ (Starkeyite) and $MgSO_4 \cdot 3H_2O$: A Revised Internally Consistent Thermodynamic Data Set for Magnesium Sulfate Hydrates. *Astrobiology* 2012;12:1042–1054.

[7] Posern K, Kaps Ch. Humidity controlled calorimetric investigation of the hydration of $MgSO_4$ hydrates. *J. Therm. Anal. Calorim.* 2008;92:905–909.

[8] Vaniman DT, Bish DL, Chipera SJ, Fialips CI, Carey JW, Feldman WC. Magnesium sulphate salts and the history of water on mars. *Nature* 2004;431:663–665.

[9] Steiger M, Linnow K, Juling H, Gülker G, Jarad A, Brüggerhoff S, Kirchner D. Hydration of $MgSO_4$-H_2O and Generation of Stress in Porous Materials. *Cryst. Growth Des.* 2008;8:336–343.

[10] van Essen VM, Zondag HA, Gores JC, Bleijendaal LPJ, Bakker M, Schuitema R, van HeldenWGJ, He Z, Rindt CCM. Characterization of $MgSO_4$ hydrate for thermochemical seasonal heat storage. *J. Sol. Energy Eng.* 2009;131:Article 041014.

[11] Marliacy P, Solimando R, Bouroukba M, Schuffenecker L. Thermodynamics of crystallization of sodium sulfate decahydrate in H_2O-NaCl-Na_2SO_4: application to $Na_2SO_4 \cdot 10H_2O$-based latent heat storage materials. *Thermochim. Acta* 2000;344:85–94.

[12] Grindrod P, Heap M, Fortes A, Meredith P, Wood I, Trippetta F, Sammonds P. Experimental investigation of the mechanical properties of synthetic magnesium sulfate hydrates: Implications for the strength of hydrated deposits on Mars. J. Geophys. Res. 2010;115: E06012.

[13] Steiger M, Linnow K, Ehrhardt D, Rohde M. Decomposition reactions of magnesium sulfate hydrates and phase equilibria in the $MgSO_4$–H_2O and Na^+–Mg^{2+}–Cl^-–SO_4^{2-}–H_2O systems with implications for Mars. *Geochim. Cosmochim. Acta* 2011;75:3600–3626.

[14] ICDD, PDF-2 Database 2001, International Centre for Diffraction Data, Newton Square, PA, USA.

[15] Janowski F, Enke E. Porous glasses. In: Schüth F, Sing KSW, Weitkamp J, editors, Handbook of porous solids, Volume 3, WILEY-VCH, Weinheim, 2002, p.1423–1542.

[16] Steiger M, Asmussen S. Crystallization of sodium sulfate phases in porous materials: The phase diagram Na_2SO_4–H_2O and the generation of stress. *Geochim. Cosmochim. Acta* 2008;72:4291–4306.

[17] Steiger M. Crystal growth in porous materials—II: Influence of crystal size on the crystallization pressure. J. Cryst. Growth. 2005;282:470–481.

[18] Steiger M, Linnow K. Phase equilibria in mesoporous materials. In: Franke L, Deckelmann G, Espinosa-Marzal R (eds): Simulation of time dependent degradation of porous materials. Cuvillier Verlag, Göttingen 2009, pp. 183–195.

[19] Chipera SJ, Vaniman DT. Experimental stability of magnesium sulfate hydrates. *Geochim. Cosmochim. Acta* 2007;71:241–250.
[20] Hamilton A, Menzies R. Raman spectra of mirabilite, $Na_2SO_4 \cdot 10H_2O$ and the rediscovered metastable heptahydrate, $Na_2SO_4 \cdot 7H_2O$. *J. Raman Spectrosc.* 2010;41:1014-1020.
[21] Wang A, Freeman JJ, Jolliff BJ. Phase transitions pathways of the hydrates of magnesium sulfate in the temperature range 50°C to 5°C. Implication for sulfates on Mars. *J. Geophys. Res.* 2009;114:E0401098.
[22] Choi BK, Lockwood DJ. Raman spcectrum of Na_2SO_4 (Phase V). *Solid State Commun.* 1989;72:133–137.
[23] Choi BK, Labbé HJ, Lockwood DJ. Raman Spectrum of Na_2SO_4 (Phase III). *Solid State Commun*. 1990;74:109-113.
[24] Linnow K, Steiger M, Lemster C, Clercq H, Jovanović M. In situ Raman observation of the crystallization in $NaNO_3$–Na_2SO_4–H_2O solution droplets. *Environ. Earth Sci.* 2013;69:1609−1620.
[25] Balboni E, Espinosa-Marzal R, Doehne E, Scherer G. Can drying and re-wetting of magnesium sulfate salts lead to damage of stone? *Environ Earth Sci.* 2011;63:1463–1473.
[26] Simonova IA, AristovYI. Sorption properties of calcium nitrate dispersed in silica gel: The effect of pore size. *Russ. J. Phys. Chem.* 2005;79:1307–1311.